Plasmonics
https://doi.org/10.1007/s11468-019-01109-2

Comparison of Fabrication Methods Based on Nanoimprinting Lithography for Plasmonic Color Filter Fabrication

Hyerin Song[1] · Won-Kyu Lee[2] · Jihye Lee[2] · Seung-Hyun Lee[3] · Young Min Song[4] · Kyujung Kim[1] · Jun-Hyuk Choi[2]

Received: 16 August 2019 / Accepted: 30 December 2019

Abstract

The angle-variable tunable optical filter was strictly fabricated by two strategies of nanoimprint-coupled metal nanopatterning with improved cost-effectiveness and accessibility. The tunable optical properties and the performances of two strategies were experimentally examined and turned out to be well matched to numerical results. Tunable properties are obtained by three factors: size of fabricated Ag nanodisks, incident illumination angle, and fabrication strategies. The resonant extinction peak shifts were identified to show a large increase along with the increase in fabricated Ag disk size and increase in the incidence angle of illumination. When comparing a fabrication strategy, it was confirmed that the sample fabricated by the strip-off method has better stability on color changes with a consistent dependency on the incident angle. The presented strategies of fabrication are technically viable for obtaining well-defined plasmonic nanostructures so that it has the feasibility to apply for fascinating optical applications including display or tunable optical filters.

Keywords Plasmonic resonance · Nanoimprint · Multilayer transfer · Optical filter · Transmittance · Nanodisks

Introduction

Subwavelength nanostructures exhibit a variety of light modulation effects, such as light interference and diffraction. Therefore, they present a new category of structural color to overcome the drawbacks of both conventional absorptive pigments and multilayered films with alternate refractive indexes. Structural color designs have been achieved based on periodic arrays of either dielectric photonic crystals [1–6] or metallic plasmonic nanostructures [7–12]. The unique optical properties of nanostructures originate from localized surface plasmon resonance (LSPR) in novel metallic nanostructures. The resonant mode of a specific structure may be sensitively tuned to the surrounding materials or configuration change. The tuning of the resonance mode can be measured with different variables and recorded to extinction, reflection, or transmission spectra [13, 14]. In several previous researches, theoretical models have been intensively investigated particularly to explain how the incident angle affects the reflective color of nanostructures [15]. These models have been widely applied for practical uses. For instance, perfect understanding of the angle-dependent property of nanostructures makes it feasible to design highly accurate and efficient tunable optical filters and sensors [16, 17].

Along with the high potential of nanostructure samples, for the commercial success of large-area nanostructure samples, more practical and higher yields are required in the fabrication process. A novel metal nanostructure is commonly fabricated by a very well-known metal lift-off method [18], which requires multiple process steps with relatively stricter and low-tolerance process optimization. Therefore, researchers have been working on fabricating corrugated nanostructures instead of strict nanostructures to reduce the effort required in fabrication, because corrugated nanostructures can easily be

Electronic supplementary material The online version of this article (https://doi.org/10.1007/s11468-019-01109-2) contains supplementary material, which is available to authorized users.

✉ Kyujung Kim
k.kim@pusan.ac.kr

✉ Jun-Hyuk Choi
junhyuk@kimm.re.kr

[1] Department of Cogno-Mechatronics Engineering, Pusan National University (PNU), Busan 46241, Republic of Korea

[2] Nanomechanical Systems Research Division, Korea Institute of Machinery and Materials (KIMM), Daejeon 34103, Republic of Korea

[3] Advanced Manufacturing Systems Research Division, Korea Institute of Machinery and Materials (KIMM), Yuseong-gu, Daejeon 34103, Republic of Korea

[4] School of Electrical Engineering and Computer Science, Gwangju Institute of Science and Technology (GIST), Gwangju 61005, Republic of Korea

Published online: 10 January 2020

fabricated using the angled evaporation method [19]. However, the performance for presenting color on corrugated structures is much inferior to that on nanostructures with strict and sharp edges because metal-free regions can be created while fabricating corrugated structures. Hence, the overall transmittance through the fabricated sample diminishes with no distinctive plasmonic resonance effect [20].

For these reasons, more efficient fabrication methods are required to fabricate nanostructures, as they are strictly designed with the specific purpose of achieving fascinating plasmonic effects. Thus, we employed the adhesive-driven metal transfer method coupled with nanoimprinting, which satisfies both the needs—high accuracy and reduced process steps. The metal transfer and strip-off methods are based on the additive and subtractive processes, respectively. Particularly, the strip-off method has been used to fabricate the multilayer metamaterial deposited inside the imprinted pattern holes and web trenches, as introduced in [21]. Both methods can generate multiple shape configurations through their process derivatives with affordable optimization criteria. Thus, they have been introduced for various research purposes or as application tools in a number of previous studies [21–24].

In this work, we attempted to fabricate nanodisks using both methods and investigated the incident angle-variable tunability of transmittance through the localized metal nanopatterned substrate. The measured transmitted spectra were employed to prove whether these schemes are effective for fabricating the strict plasmonic metal nanostructures with the distinctive angle-variable transmittance property. The measurement scheme of angle-variable transmittance spectra is almost similar to the reference works [20–22]. The tuning of optical properties was experimentally confirmed by the resonant peak shifts resulting from the various incident angles, sizes, and periodicities of the fabricated nanopatterns. In addition, a numerical analysis was conducted to theoretically support the obtained tuning transmissive optical properties.

Methods

Experiments

For both the additive metal transfer and subtractive strip-off applied in this work, the nanoimprint master pattern is prepared at the first step of the metal nanopattern fabrication. Four different designs were implemented—150-nm, 200-nm, 250-nm, and 400-nm hole diameter in either hexagonal array with their pitch equal to twice its hole diameter. The silicon master patterns for nanoimprinting were fabricated by KrF optical lithography, followed by a properly controlled anisotropic etching at the National Nanofab Center in Daejeon, Korea. They were replicated in UV curable mold resin (RM311 from Changseung Sheets Inc., Republic of Korea) on PET film, which was followed by an anti-stiction surface treatment by the vapor deposition of trichloro(1H,1H,2H,2H-perfluorooctyl)silane (Sigma-Aldrich, St. Louis, MO, USA) to conservatively facilitate the mold release in the later process steps. The replicated mold with the reversed phase of pattern configuration was used either for UV nanoimprinting followed by the metal deposition, silver in this work, onto the imprinted pattern for the metal strip-off, or for silver deposition directly onto the replicated mold for metal transfer.

Figure 1 a illustrates the metal strip-off process from the UV nanoimprinted pattern onto the spin-coated resin (NIL0210, MRT GmbH, Germany), whereas Fig. 1 b shows the metal transfer process from the replicated mold pattern. The SEM images exhibited the evidently reversed pattern profile owing to the different number of replications. On the imprinted pattern surface, a 30-nm-thick silver layer was deposited by the custom-made e-beam evaporator. At this stage, the nanopatterned surface is chemically treated to minimize the adhesion force with the abovementioned surface treatment methods to ensure that the deposited metal layer can be stripped off easily. The metal strip-off process follows the previously reported optimized process condition [25]. Epoxy-based ultraviolet (UV) curable resin (NOA 61; Norland Inc., Fort Atkinson, WI, USA) coated on a flexible PET film was partially cured by UV exposure at an energy of 9 mJ (approximately 50% of its complete cure energy) prior to being used as an adhesive layer. Excessive pre-curing would lead to near solidification with diminished adhesion, whereas insufficient UV exposure will cause complete removal of the whole layer of the deposited silver including those in the trench. The optimized pre-cure was expected to remove the Ag layer only from the raised surface of the nanopatterns, which resulted in the transferred silver layer with open-hole regions in the adhesive layer, as depicted in Fig. S1 (c-1). Finally, the silver disks only inside the imprinted-hole regions remained after stripping off, as depicted in Fig. S1 (c-2).

The metal transfer process illustrated in Fig. 1 b is quite similar to the strip-off process except for the need to control the embedded depth of the metal and the corresponding structure configuration. A thinner adhesive layer (mrI-6000E.1, MRT Inc., Germany, ~ 100 nm in layer thickness) compared to that used for metal strip-off was applied because of its better suitability and ease of making the embedded depth consistent and improving process reliability. At mild temperatures of approximately 40 °C, the contact press by approximately 10–20 kPa caused conformal sticky contacts with the Ag layer on the protruded surface of the mold nanopatterns. Subsequently, the complete UV cure and mold release created the transferred Ag disks in the adhesive layer, as shown in Fig. S1 (f-1), and the Ag layer inside the recessed region still remained, as shown in Fig. 1 (f-2). Hence, Fig. S1 (c-2) and Fig. 1 (f-2) represent patterns made by the strip-off and

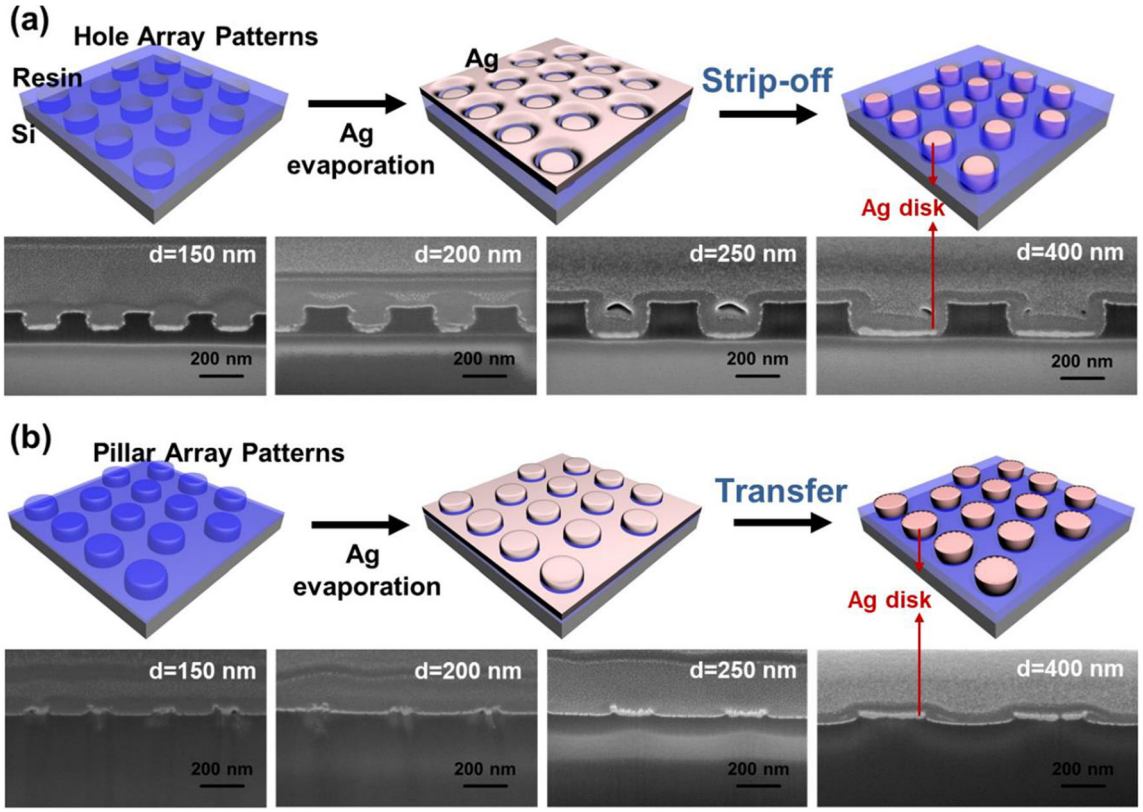

Fig. 1 Schematic images of fabrication process: **a** strip-off method and **b** transfer method. The fabricated structures with different diameters of Ag disks are shown in the XZ-planar cross-sectional SEM images under the schematic images that show the fabrication process

transfer process, respectively, indicated by the finalized samples on a 2-in. glass substrate. Their structural configuration was examined by a FIB (focused ion beam) (NOVA200, FEI, located in the National Nanofab Center), particularly for their sidewall profiles. The measurement scheme comprised the detector and the illumination aligned in a straight line, and the fabricated sample held by the rotation stage located in between them, as in [26, 27]. The angle-variable transmittance spectroscopy was measured in the region of UV–Vis to NIR range with a spectrophotometer (S3100, SCINCO, Republic of Korea/U-4100, Hitachi, Japan).

Numerical Analysis

The experimental data was verified and qualitatively discussed with the assistance of modeling and simulation using the rigorous coupled-wave analysis (RCWA). The wavelength-dependent optical properties for silver were taken from the database reported by Johnson and Christy [28]. The refractive index value of the resin was set as 1.52, as given by the product dataset. The experimental factors, specifically the dimensional parameters of shape and periodicity, and the size of nanostructures were derived using scanning electron microscopy (SEM) images of the samples, and those were maximally incorporated into the modeling process for numerical analysis. The formational factors, such as the size, thickness, pattern depth, periodicity, and edge curvature, were picked up empirically to be carefully considered in the numerical analysis. The results were moderated through the Gaussian function for clearly finding the peaks by minimizing the fluctuations in the spectra.

Results and Discussion

The cross-sectional profiles of the samples created by the strip-off and transfer methods were comparatively analyzed via FIB-machined SEM for the pattern master of hole diameter 150 nm to 400 nm, as presented in Fig. 1. First, the samples obtained from the strip-off method maintain the nanoimprinted structure profile, apparently with the deposited Ag layer into the recessed regions. The bright layer around the structure skin is a 10-nm-thick Pt layer coated prior to loading the sample into the FIB, and the deposited Ag layer remained inside the trench. It was also confirmed that the Ag layers on the top surface of the nanoimprinted patterns were properly removed. On the other hand, the samples for transfer showed different configurations, as shown in Fig. 1 b. The transferred Ag nanodisks seemed to be slightly embedded into the adhesive layer without forming the imprinted structure profile.

Therefore, the effect of the diffractive interference owing to the phase change was minimized.

The corresponding transmittance spectroscopy was measured at various incidence angles and the obtained data are presented in Fig. 2 a for the strip-off sample and Fig. 2 b for the transfer sample, both of which have 200-nm-diameter Ag disks incorporated in the array. These samples were fabricated from the nanoimprint pattern master with a hole diameter of 200 nm, pitch equal to twice the diameter, and 150 nm in hole depth via either the strip-off or the transfer method. The presenting color through the patterned substrates at several angles, by rotating the sample to apply the light at different incidence angles, was captured as the image data and shown in Fig. 2. The gradual color change of green to blue appears evidently as the angle increases and it is proved through angle-variable transmittance spectra in Fig. 2, when other factors such as diameter and periodicity of Ag disks are fixed as 200 nm and 400 nm, respectively. As shown in the spectra, the following observations were made. From the strip-off method, it was observed that the plasmonic resonant peaks are located at approximately 800 nm, but from the transfer method, they were observed to be at approximately under 700 nm with 200-nm-diameter Ag disks array at normal incidence. The practically obtained transmittance spectra using the fabricated samples at various diameters, periodicities, and angle dependencies are presented in Fig. S2 and Fig. S3, which represent the results measured on the samples using the strip-off and transfer methods, respectively. Referring to the measurement data shown in Fig. S2 and Fig. S3, generally, the resonance peak wavelength was observed to be shorter for the transfer sample by approximately 100 nm than the strip-off sample, which probably implies that the imprinted depth affects the embedded depth of the Ag nanodisks and subsequently the resonance extinction. Second, the silver disk size dominantly affects the resonant peak position. At normal illumination and zero-order optical detection, the resonance peak wavelength for the sample fabricated by the strip-off method shifted from 690 to 1352 nm as the silver disk size increased from 150 to 400 nm, whereas it increased from 576 to 1256 nm for the sample fabricated by the transfer method. The resonance shifts were even increased when measuring at the angled illumination. Third, the illumination angle was also proven to affect the plasmonic resonance significantly, and consequently, the spectral transmittance property changes. At a higher tilted angle, the resonant peak wavelength got red-shifted, the ratio of which depended on the silver disk size (or hole diameter) in proportion. This is true of both the samples. Most significantly, we confirmed that the sample fabricated by the strip-off method has better stability on color changes with a consistent dependency on the incident angle. The sample fabricated by the transfer method loses a clear resonance peak gradually as the incident angle is increased. After all, the resonance peak vanishes beyond the threshold incident angle, whereas the resonance peak is clearly observed for the sample fabricated by the strip-off method. This tendency seems to be sustained well in the strip-off sample rather than in the transfer sample, particularly with small disk size samples.

To clearly understand the tendency, the amount of the resonant peak shifts in the transmission spectra shown in Fig. S2 and Fig. S3 is calculated and plotted in Fig. 3. The values were obtained by subtracting the value of wavelength measured at 0° from the value of wavelength measured at the angled position. It means that each point represents a relative resonant wavelength position from a resonance peak position at normal incidence. To clarify the number of peak shifts, a linear fitting was done and plotted with solid lines. According to Fig. S2

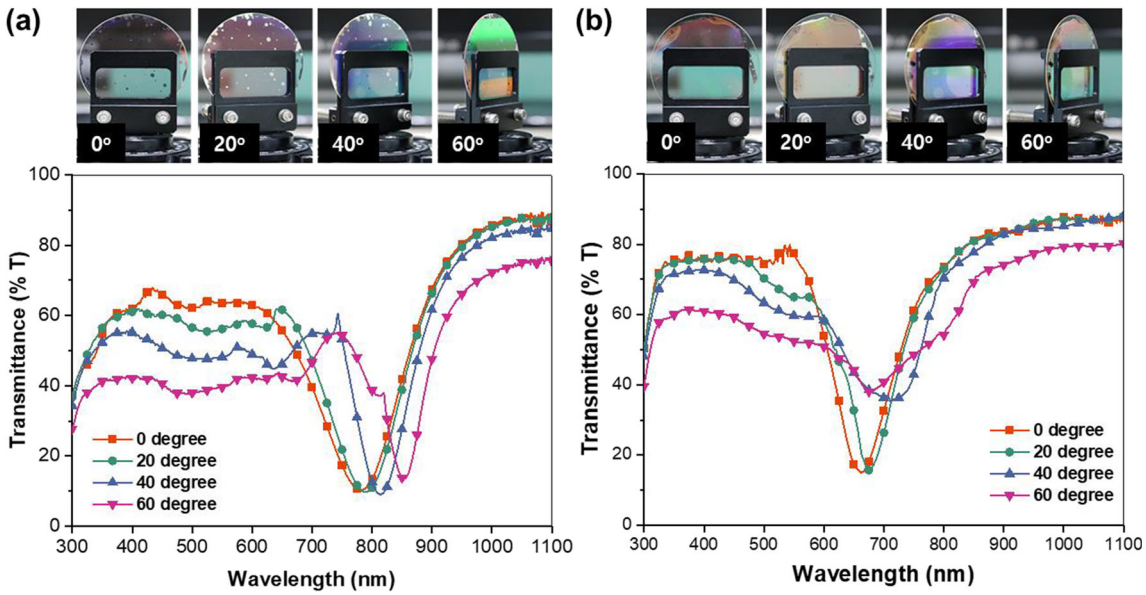

Fig. 2 The measured angle-dependent transmittance images and spectra at the diverse incidence angles with the fabricated 200-nm-diameter Ag disks via **a** strip-off and **b** transfer methods

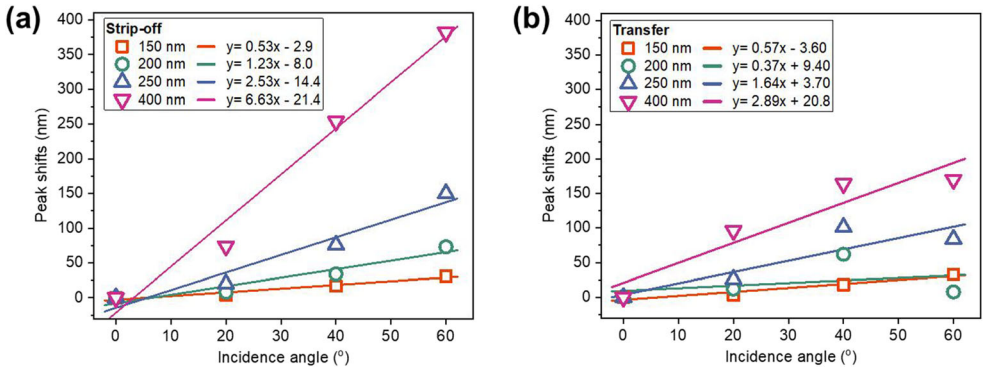

Fig. 3 Obtained resonance peak shifts in transmission spectra measured with the fabricated **a** strip-off sample substrates and **b** transfer sample substrates when the incidence angle changes from 0° to 60°. Effects of the diameters of the Ag nanodisks also are presented. Each point represents a wavelength at the resonance mode, and the peak shifts in *y*-axis were calculated by setting the value of wavelength measured at 0° as reference. The linear fitted results are shown with solid lines

(a), the resonance peak position of the 150-nm-diameter Ag patterns fabricated by the strip-off method is 690 nm and shifts to 1352 nm when measured with 400-nm-diameter Ag disks. This means that the size-driven wavelength shift is estimated to be 662 nm at normal incidence and 1013 nm at 60° incidence. The angle-dependent wavelength shifts increased from 31 up to 382 nm with the diameter of Ag disks from 150 to 400 nm, at which the optical properties are affected critically by the silver disk size. A similar trend occurred in the transfer samples shown in Fig. S3. The angle-dependent shifts of the peak resonant wavelength were in the range 33–170 nm, so that the size-driven resonant wavelength shifted from 680 nm at normal incidence to 817 nm at 60° tilt incidence. There is a slight difference in the angle-variable wavelength shift range between the two process schemes. Although the qualitative angle-variable behavior showed similar tendency, a narrower shift range was observed for the transfer samples. This can be explained in relation to the shorter resonant extinction wavelength for the transfer samples than for the strip-off ones probably owing to the coupled structural property. In addition, the transmittance at the resonant wavelength is of interest to discuss comparatively. Fig. S2 exhibited much lower extinction transmittance at the smaller disk size, 9.2% average transmittance with a 150-nm-diameter disk in the strip-off sample, and it sustained as the disk size grew. However, the transmittance through the transfer sample was approximately 28%, and it became less as the disk size grew. When comparing Fig. S2 and Fig. S3, the strip-off samples seem to provide clearer and distinctive spectral configuration than the transfer samples, in general. To figure out its dependence on the illumination angle for both process schemes shown in Fig. S2 and Fig. S3, the simulation was performed to supplement the measurements.

It is of significance to analytically deduce the shift of the resonant extinction wavelength with respect to disk size and illumination angle and the difference between strip-off and transfer owing to the structural configurations. In Fig. 4, the calculated spectral data depending on the aforementioned factors are presented: (a) is the transmittance spectra for the strip-off samples and (b) is that for the transfer samples. The graphs in the second column in Fig. 4 present the contoured transmittance spectroscopy in terms of incidence angle for the two selected sizes of Ag disks and both the process schemes, respectively. The color bar represents the transmittance—purple to red color variations represent 0 to 100%. The other data obtained with the 250-nm- and 400-nm-diameter Ag nanodisks are presented in Fig. S4. The last column in Fig. 4 shows the outcome number of peak shifts at the resonance mode as the tilt angle increased from normal incidence according to the calculation data. The tendencies of calculated results match well with the measured data shown in Fig. S2 and S3, satisfying our expectation. The size and periodicity dependence of LSPR on the nanostructures has already been well reported through previous researches even recently [29, 30] and it should be noticed that the outcome calculation confirms the effect well, even the slight broadening of the SP band. The Ag disks in the strip-off samples are surrounded by resin whereas those in the transfer samples are exposed to air. Because the former is governed more by the higher refractive index in the surrounding material, a longer wavelength of the resonant peak occurred for the strip-off sample. Referring to the SP band position obtained from the result, we could determine the relevance between the size of nanodisks and the position of the resonance peak; as the size of Ag disks increased, the resonance peak shifted to the longer wavelength region. Furthermore, it was verified that the changes in incidence angle resulted in the red shift of the SP band. The angle-dependent red shifts could be explained by the changes in the aspect ratio of the Ag nanodisk. In this research, incident light was applied at various angles to the nanodisk-patterned substrate. Thus, the aspect ratio of the Ag nanodisks embedded in the resin structure varied from 1:1 to 1:2 toward the illumination direction in accordance with the incidence angle changing from 0° to 60° as the sample was turned. Correspondingly, the incident light travels a higher aspect ratio of the nanodisks as

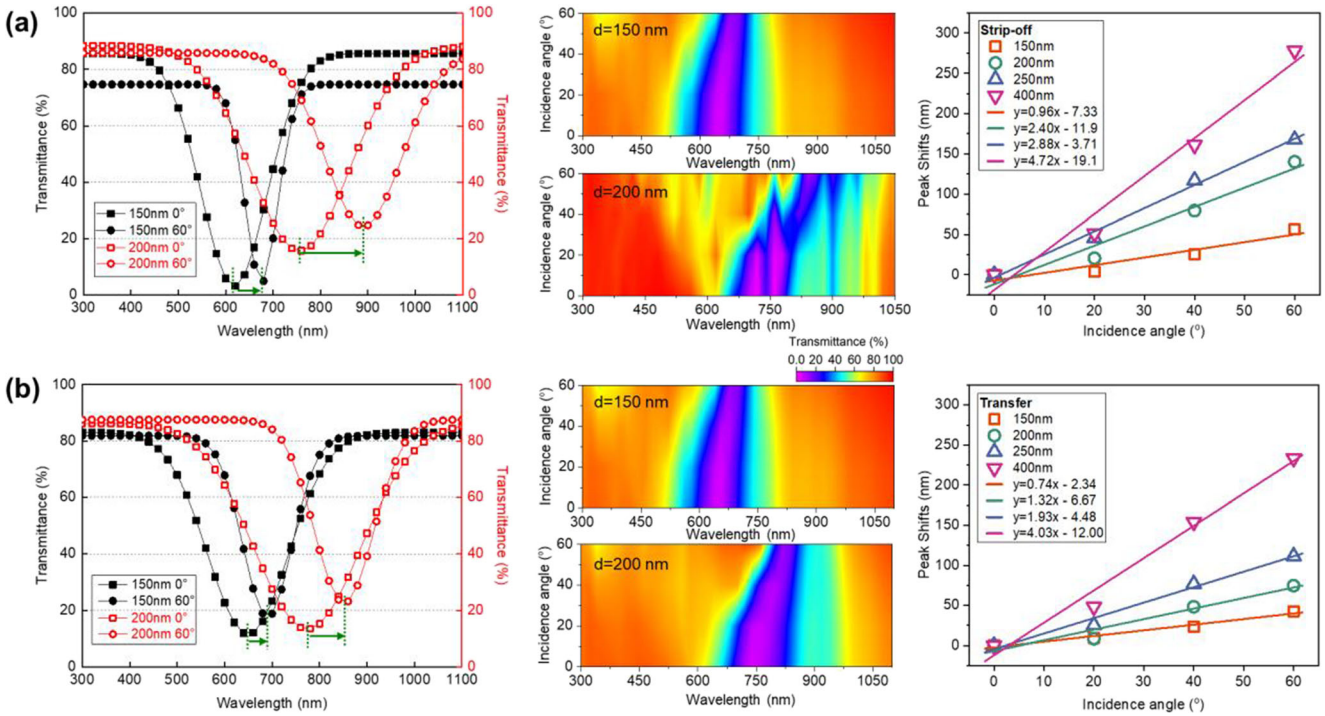

Fig. 4 Calculated transmission spectra with **a** a strip-off sample and **b** a transfer sample depending on the following factors: (1) diameter of Ag nanodisk and (2) incident angle. The resonance peak shifts in transmission spectra from simulation data are presented in the last column

the incident angle increased, which implies that the dipolar moments of the nanodisks result in multipolar resonance. In previous research, it was proven that the extinction peaks of nanodisks moved to longer wavelengths for larger aspect ratios [25, 31, 32]. This can explain analytically that the incidence angle can cause the shift of the extinction peak wavelength via the change of structural profile in the illumination direction. Furthermore, the refractive index of the surrounding material near the structure can sensitively affect the extinction peak, and the shifts are enlarged at the higher aspect ratio of the nanohole structure [32]. Consequently, the largest peak shifts were found in the 400-nm-diameter Ag disks surrounded by resin, which is fabricated by the strip-off process. The tendency increased along with the increment of the Ag disk size, which was presented well in the last column in Fig. 4. The slopes of the solid lines reflect the extent to which the optical properties are affected by the given parameters. Similar to the measured data, all the slopes for strip-off samples are larger than those for the transfer samples under the same conditions.

Conclusion

Two fabrication strategies based on adhesive layer–assisted peel-off were devised to enable efficient metal nanopatterning with improved cost-effectiveness and accessibility. The fabricated nanopatterns were exploited to prove the efficiency of strategies in fabricating a desired structure. Furthermore, the angle-variable transmittance property was examined to validate tunable optical performance and we compared the performance based on both strategies for examining the feasibility of the product as an angle-dependent wavelength filter. The strip-off method produced Ag nanodisks only in the recessed regions, whereas the transfer process produced silver disks embedded slightly into the adhesive layer. The difference in their structural profiles with or without the presence of the nanoimprinted holes resulted in their corresponding complex photonic properties. For the given test samples having four different hole diameters, with their periodicity almost twice of the diameters, the measured transmittance spectroscopy data at varying incidence angles were presented along with their counterpart numerical analysis.

The measured spectra show remarkably distinctive spectral modes depending on the configurations of the samples, which matched well with the numerical results. This proves that the attempted fabrication strategies worked well to produce the strict configurations of nanodisks. Summarizing the analysis on the tuning performance with the measurement data, the resonant peak wavelength clearly red-shifted with increase in angle tilting and Ag disk size for the patterned substrates fabricated using both strategies. The largest size-variable resonance peak shift was observed in the range of 817 to 1013 nm from the normal to 60° incidence angle with the strip-off sample. The resonant peak shift achieved by the incident angle and Ag disk size were also supported by the

carried out calculated results and both results are in good agreement. According to the calculated data with strip-off samples, approximately 882 nm of resonance peak shift can be achieved at 60° incidence angle by changing the disk size from 150 to 400 nm, and up to 278 nm of resonance peak shift can be achieved as the incidence angle varies. The resonance peak responds to the increased effective refractive index value owing to the presence of the imprinted structure profile and the resin over the nanodisk array, resulting in peak shifts. The resonant peak wavelength was found to be longer by more than 100 nm for the strip-off sample than for the transfer sample, which can lead us to infer that the imprinted structure profile was affected optically by the increased effective refractive index value owing to a surrounding resin. The resonant extinction transmittances were identified to show a larger increase along with the Ag disk size proportionally for the strip-off sample as compared to the transfer sample. The presented strategies of fabrication are technically viable and cost-effective with improved accessibility for obtaining a well-defined plasmonic nanostructure, in comparison with the increased number of the process steps demanded in the conventional metal lift-off and adopting costly modern advanced photolithography line-up. Hence, it can be potentially applicable to fascinating optical applications including displays or optical filters and affordable as well.

Funding information This research was supported by the National Research Foundation of Korea (NRF) funded by the Ministry of Science and ICT (2018R1A4A1025623, 2017M3D1A1039287). In addition, this research was funded by the Korea Institute for Advancement of Technology (KIAT) (N0002310) under the Ministry of Trade, Industry, and Energy (MOTIE).

Compliance with Ethical Standards

Conflict of Interest The authors declare that they have no competing interests.

References

1. Kanamori Y, Shimono M, Hane K (2006) Fabrication of transmission color filters using silicon subwavelength gratings on quartz substrates. IEEE Photon Technol Lett 18:2126–2128
2. Cho E-H, Kim H-S, Cheong B-H et al (2009) Two-dimensional photonic crystal color filter development. Opt Express 17:8621
3. Kinoshita S, Yoshioka S, Miyazaki J (2008) Physics of structural colors. Rep Prog Phys 71:076401
4. Kim H, Ge J, Kim J et al (2009) Structural colour printing using a magnetically tunable and lithographically fixable photonic crystal. Nat Photonics 3:534
5. Kim W-G, Song H, Kim C et al (2016) Biomimetic self-templating optical structures fabricated by genetically engineered M13 bacteriophage. Biosens Bioelectron 85:853–859
6. Kim W-G, Kim K, Ha S-H et al (2015) Virus based full colour pixels using a microheater. Sci Rep 5:13757
7. Xu T, Shi H, Wu Y-K, Kaplan AF, Ok JG, Guo LJ (2011) Structural colors: from plasmonic to carbon nanostructures. Small 7:3128–3136
8. Xu T, Wu Y-K, Luo X, Guo LJ (2010) Plasmonic nanoresonators for high-resolution colour filtering and spectral imaging. Nat Commun 1:59
9. Kaplan AF, Xu T, Jay Guo L (2011) High efficiency resonance-based spectrum filters with tunable transmission bandwidth fabricated using nanoimprint lithography. Appl Phys Lett 99:143111
10. Yokogawa S, Burgos SP, Atwater HA (2012) Plasmonic color filters for CMOS image sensor applications. Nano Lett 12:4349–4354
11. Laux E, Genet C, Skauli T, Ebbesen TW (2008) Plasmonic photon sorters for spectral and polarimetric imaging. Nat Photonics 2:161
12. Lee H-S, Yoon Y-T, Lee S-S et al (2007) Color filter based on a subwavelength patterned metal grating. Opt Express 15:15457–15463
13. Ahn H, Song H, Shin D-M et al (2018) Emerging optical spectroscopy techniques for biomedical applications—a brief review of recent progress. Appl Spectrosc Rev 53:264–278
14. Song H, Ahn H, Kim T et al (2019) Manipulation of light at the nanoscale for high-performance spectroscopic and optical applications. Appl Spectrosc Rev 54:482–508
15. Ahn H, Song H, Choi J-R, Kim K (2017) A localized surface plasmon resonance sensor using double-metal-complex nanostructures and a review of recent approaches. Sensors 18:98
16. Lochbihler H (2015) Polarizing and angle-sensitive color filter in transmittance for security feature applications. Adv Optical Technol 4:12155
17. Davis MS, Zhu W, Xu T et al (2017) Aperiodic nanoplasmonic devices for directional colour filtering and sensing. Nat Commun 8:1347
18. Arslan D, Chong KE, Miroshnichenko AE et al (2017) Angle-selective all-dielectric Huygens' metasurfaces. J Phys D Appl Phys 50:434002
19. Duempelmann L, Casari D, Luu-Dinh A, Gallinet B, Novotny L (2015) Color rendering Plasmonic aluminum substrates with angular symmetry breaking. ACS Nano 9:12383–12391
20. Sauvage-Vincent J, Tonchev S, Veillas C et al (2013) Optical security device for document protection using plasmon resonant transmission through a thin corrugated metallic film embedded in a plastic foil. Journal of the European Optical Society - Rapid publications 8
21. Jeon S, Sung S-K, Jang E-H et al (2018) Multilayer metal-oxide-metal nanopatterns via nanoimprint and strip-off for multispectral resonance. Appl Surf Sci 428:280–288
22. Xin JZ, Lee FK, Li SYW et al (2011) Transfer imprint lithography using a soft mold. Microelectron Eng 88:2632–2635
23. Gao L, Shigeta K, Vazquez-Guardado A, Progler CJ, Bogart GR, Rogers JA, Chanda D (2014) Nanoimprinting techniques for large-area three-dimensional negative index metamaterials with operation in the visible and telecom bands. ACS Nano 8:5535–5542
24. Jeong JW, Yang SR, Hur YH et al (2014) High-resolution nanotransfer printing applicable to diverse surfaces via interface-targeted adhesion switching. Nat Commun 5:5387
25. Jun TAO, Yong-Hua LU, Rong-Sheng Z et al (2008) Effect of aspect ratio distribution on localized surface plasmon resonance extinction spectrum of gold nanorods. No 12:4459
26. Si G, Zhao Y, Leong ESP et al (2014) Incident-angle dependent color tuning from a single plasmonic chip. Nanotechnology 25:455203
27. Zheng J, Ye Z-C, Sheng Z-M (2016) Reflective low-sideband plasmonic structural colors. Opt Mater Express, OME 6:381–387
28. Johnson PB, Christy RW (1972) Optical constants of the noble metals. Phys Rev B Condens Matter 6:4370–4379

29. Zorić I, Zäch M, Kasemo B, Langhammer C (2011) Gold, platinum, and aluminum nanodisk plasmons: material independence, subradiance, and damping mechanisms. ACS Nano 5:2535–2546
30. Ye M, Sun L, Hu X, Shi B, Zeng B, Wang L, Zhao J, Yang S, Tai R, Fecht HJ, Jiang JZ, Zhang DX (2015) Angle-insensitive plasmonic color filters with randomly distributed silver nanodisks. Opt Lett 40:4979–4982
31. Chung T, Lee S-Y, Song EY, Chun H, Lee B (2011) Plasmonic nanostructures for nano-scale bio-sensing. Sensors 11:10907–10929
32. Hanarp P, Käll M, Sutherland DS (2003) Optical properties of short range ordered arrays of nanometer gold disks prepared by colloidal lithography. J Phys Chem B 107:5768–5772